



HAL
open science

Nonparametric test for connectivity detection in multivariate autoregressive networks and application to multiunit activity data

Matthieu Gilson, A. Tauste Campo, X. Chen, A. Thiele, G. Deco

► **To cite this version:**

Matthieu Gilson, A. Tauste Campo, X. Chen, A. Thiele, G. Deco. Nonparametric test for connectivity detection in multivariate autoregressive networks and application to multiunit activity data. *Network Neuroscience*, 2024, 1 (4), pp.357 - 380. 10.1162/netn_a_00019 . hal-04449913

HAL Id: hal-04449913

<https://amu.hal.science/hal-04449913>

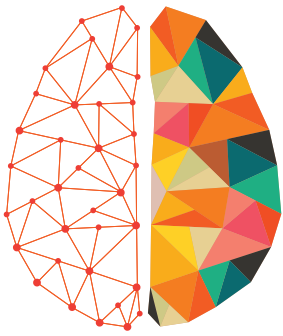
Submitted on 9 Feb 2024

HAL is a multi-disciplinary open access archive for the deposit and dissemination of scientific research documents, whether they are published or not. The documents may come from teaching and research institutions in France or abroad, or from public or private research centers.

L'archive ouverte pluridisciplinaire **HAL**, est destinée au dépôt et à la diffusion de documents scientifiques de niveau recherche, publiés ou non, émanant des établissements d'enseignement et de recherche français ou étrangers, des laboratoires publics ou privés.



Distributed under a Creative Commons Attribution 4.0 International License



NETWORK NEURO SCIENCE

an open access  journal



Citation: Gilson, M., Tauste Campo, A., Chen, X., Thiele, A., & Deco, G. (2017). Nonparametric test for connectivity detection in multivariate autoregressive networks and application to multiunit activity data. *Network Neuroscience*, 1(4), 357–380. https://doi.org/10.1162/netn_a_00019

DOI:
https://doi.org/10.1162/netn_a_00019

Supporting Information:
<http://www.scipy.org>
<http://dally.nimh.nih.gov/index.html>

Received: 3 January 2017
Accepted: 1 June 2017

Competing Interests: The authors have declared that no competing interests exist.

Corresponding Authors:
Adria Tauste Campo
adria.tauste@upf.edu
Matthieu Gilson
matthieu.gilson@upf.edu

Handling Editor:
Pedro Valdes-Sosa

Copyright: © 2017
Massachusetts Institute of Technology
Published under a Creative Commons
Attribution 4.0 International
(CC BY 4.0) license



METHODS

Nonparametric test for connectivity detection in multivariate autoregressive networks and application to multiunit activity data

M. Gilson¹, A. Tauste Campo^{1,2}, X. Chen³, A. Thiele³, and G. Deco^{1,4}

¹Computational Neuroscience Group, Departament de Tecnologies de la Informació i les Comunicacions, Universitat Pompeu Fabra, Barcelona, Spain

²Epilepsy Monitoring Unit, Department of Neurology, Hospital del Mar Medical Research Institute, Barcelona, Spain

³Institute of Neuroscience, Newcastle University, Newcastle upon Tyne, United Kingdom

⁴Institució Catalana de Recerca i Estudis Avançats, Barcelona, Spain

Keywords: Network connectivity detection, Nonparametric significance method, Multivariate autoregressive process, Granger causality, Multiunit activity

ABSTRACT

Directed connectivity inference has become a cornerstone in neuroscience to analyze multivariate data from neuroimaging and electrophysiological techniques. Here we propose a nonparametric significance method to test the nonzero values of multivariate autoregressive model to infer interactions in recurrent networks. We use random permutations or circular shifts of the original time series to generate the null-hypothesis distributions. The underlying network model is the same as used in multivariate Granger causality, but our test relies on the autoregressive coefficients instead of error residuals. By means of numerical simulation over multiple network configurations, we show that this method achieves a good control of false positives (type 1 error) and detects existing pairwise connections more accurately than using the standard parametric test for the ratio of error residuals. In practice, our method aims to detect temporal interactions in real neuronal networks with nodes possibly exhibiting redundant activity. As a proof of concept, we apply our method to multiunit activity (MUA) recorded from Utah electrode arrays in a monkey and examine detected interactions between 25 channels. We show that during stimulus presentation our method detects a large number of interactions that cannot be solely explained by the increase in the MUA level.

INTRODUCTION

In recent years, there has been a growing interest in developing multivariate techniques to infer causal relations among time series. The initial formulation of the problem goes back to the seminal work by Granger in the 1960s (Granger, 1969) motivated by the analysis of the pairwise influence between economic time series. In this work, Granger decomposes the cross-spectrum of two autoregressive time series into two directional components that account for the potential causal influences between each other. A general solution of the problem in multivariate scenarios was developed a decade later by the introduction of multivariate autoregressive (MVAR) processes, which allow the estimation of causal relationships between nodes in networks with linear feedback based on their observed activity (Amemiya, 1974; Geweke, 1982, 1984; Lütkepohl, 2005). The MVAR was further combined with spectral analysis to develop the directed transfer entropy function (Kaminski & Blinowska, 1991; Kamiński, Ding, Truccolo, & Bressler, 2001), which has been employed to analyze

Noise-diffusion network:
Stochastic model used in statistics to capture linear interactions among multiple time series.

Granger causality analysis:
Estimation of directional interactions between time series from the residuals of two MVAR linear regressions.

Error residuals:
Unexplained variability of the node activity in a multivariate process (e.g., MVAR) fitted to observed time series.

Parametric and nonparametric significance testing:
Comparison of estimated value with a known (parametric) or surrogate (nonparametric) reference probability distribution.

connectivity patterns in neurobiological systems (Babiloni et al., 2005; Wilke, Ding, & He, 2008). Granger causality analysis is nowadays often used to evaluate the influence of a group of variables onto another, which corresponds to the influence of a subgroup of nodes onto another one in networks. In particular, it is also applied to detect individual connections between pairs of nodes (each subgroup being a single node), which sets the context of the present paper.

In neuroscience, this inference problem has been transposed to analyze interactions between neuronal populations from spiking activity or neuroimaging measurements such as fMRI, EEG, and MEG (Lusch, Maia, & Kutz, 2016; Messé, Rudrauf, Benali, & Marrelec, 2014; Michalareas, Schoffelen, Paterson, & Gross, 2013; Rogers, Katwal, Morgan, Asplund, & Gore, 2010; Seth, Barrett, & Barnett, 2015; Storkey et al., 2007). Two types of estimation procedures may be distinguished: measures relying on an underlying interaction model such as Granger causality analysis (M. Ding, Chen, & Bressler, 2006) and dynamic causal modeling (DCM) (Friston, Harrison, & Penny, 2003) on the one hand; and model-free measures such as transfer entropy (Schreiber, 2000) and directed information (Massey, 1990), which make minimal model assumptions, on the other hand. Although model-free approaches have proven useful to describe neural propagation at spike-train level (So, Koralek, Ganguly, Gastpar, & Carmena, 2012; Tauste Campo et al., 2015), certain assumptions are required when estimating interactions at the neuronal population level, in which broader spatial and temporal scales contribute to shaping the signals. Motivated by data-driven practical problems, methodological refinements of Granger causality analysis (or MVAR-based methods) have considered additive noise (Vinck et al., 2015) or measurement noise via state-space models (Barnett & Seth, 2015; Friston et al., 2014). However, in the majority of cases, the ratio behind the detection test concerns submodel error residuals, which might become too similar when connections are placed in a highly redundant network, thus increasing the missed detection rate (Stramaglia, Cortes, & Marinazzo, 2014).

To detect directed connections in the general context of large networks, we propose to test the significance of the MVAR coefficients using a nonparametric procedure. As a generative model, the MVAR process is canonically related to Granger causality analysis: the linear regression in the upper right inset of Fig. 1A provides both coefficients and residuals, the latter being viewed as the remaining uncertainty in the prediction of the target time series by its source(s). By comparing the residuals of two linear regressions—one involving a supposed driver node and one without it—in a log ratio, traditional tests for Granger causality estimate the effective interaction of one node onto another (Barrett & Barnett, 2013). Since these log ratios asymptotically converge to known distributions, parametric statistical tests have been developed to assess the significance of these interactions (Barnett & Seth, 2014). Instead, our proposed method evaluates the significance of the MVAR coefficients to infer the existence of network connections. To achieve this, we propose a nonparametric significance test in the regression coefficients space. Previous literature on nonparametric testing for Granger causality has resorted to surrogate data generated by trial shuffling (Dhamala, Rangarajan, & Ding, 2008; Nedungadi, Rangarajan, Jain, & Ding, 2009), bootstrap procedures (Diks & DeGoede, 2001), or phase randomization in frequency-domain measures (L. Ding, Worrell, Lagerlund, & He, 2007; Li et al., 2016). Here we focus on within-trial surrogate tests for time-domain coefficients as done in previous studies (Faes, Marinazzo, Montalto, & Nollo, 2014; Schreiber & Schmitz, 1996; Winkler, Ridgway, Webster, Smith, & Nichols, 2014).

Our approach is motivated by the growing of multichannel recording techniques in neuroscience, which require tailored multivariate analysis. In the context of recurrent networks,

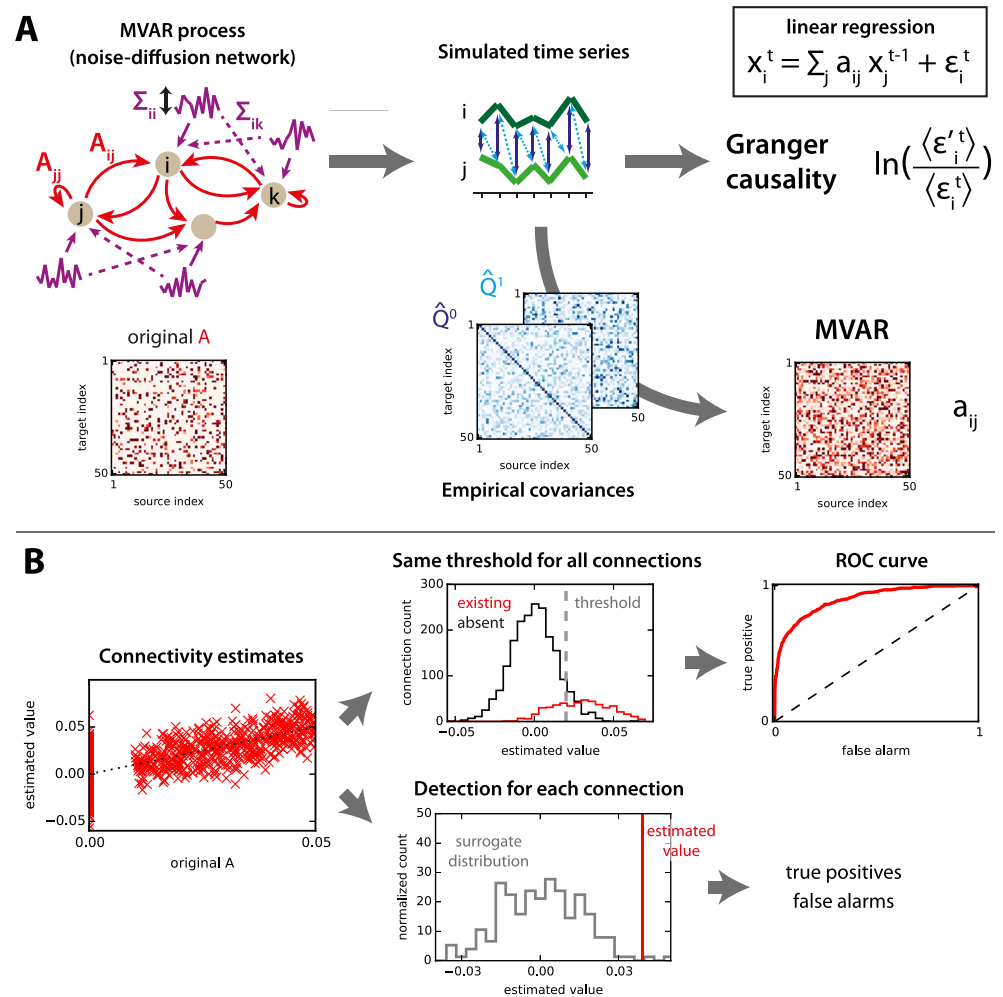


Figure 1. Network model and connectivity estimation. (A) For a given directed connectivity A and input covariances Σ (left), the network activity (middle) is simulated using Equation 1. From the observed time series, the existing interactions in the original connectivity can be estimated (right): Granger causality analysis uses the residuals of linear regressions (ϵ in the upper right equation; see Methods for details about the residuals used in the log ratio), whereas MVAR corresponds to the coefficients. Note that MVAR can be obtained using the empirical covariance matrices \hat{Q}^0 and \hat{Q}^1 ; see in Equation 7 for $\tau = 0$ and 1. (B) The left panel compares the estimated values with the original values for all connections in the network. The upper thread displays the distributions of estimated values for existing and nonexisting connections in the original network. Using a sliding threshold (vertical dashed gray line) on the estimated values, one can calculate the ROC curve (right). The lower thread compares the estimated value for a single connection with a null distribution. From this, the choice of whether the connection exists is made for each individual connection.

False alarm (or false positive): Wrong rejection of the null hypothesis in a detection test (here detecting a connection that is absent in the original connectivity).

which are ubiquitous in neuroscience, we provide numerical evidence that these tests can achieve a good control of the false-alarm rate and might improve the miss rate by properly adapting the null distribution to each connection. The focus of the present analysis is on the case where we observe more time samples (a few thousands per node) than the network size (about a hundred nodes), a usual ground for electrophysiological data. Within this regime, we test the robustness of the detection method for a broad range of network parameters and various nontrivial topologies inspired by neuronal networks.

Multivariate autoregressive (MVAR) process:
Dynamic network model where nodes linearly interact between each other while receiving input noise; in discrete time, this definition is mathematically equivalent to the MVAR process.

METHODS: MULTIVARIATE AUTOREGRESSIVE MODEL AND CONNECTIVITY ESTIMATION

The activity in the MVAR process—also known as noise-diffusion discrete-time network—is described by the following equation:

$$x^t = Ax^{t-1} + \zeta^t, \tag{1}$$

where the connection matrix A describes the interactions between coordinates of the vector $x^t = (x_i^t)$ with time t being an integer and node index $1 \leq i \leq N$. Here we constrain our study to the case where ζ^t is Gaussian (possibly cross-correlated noise), whose realizations are time independent for successive time steps. Without loss of generality, we assume that all variables ζ^t are zero mean. We only consider MVAR processes of order 1 in a first place, but will extend the work to the case of order 2 in a later section.

Granger Causality Analysis

Granger causality analysis is usually presented using time series, and the estimation of nonzero coefficients in A from observed activity over a period $1 \leq t \leq T$ relies on the linear regression of the activity x_i^t of a given node i at time t by the past activity of a subset \mathcal{S} of network nodes:

$$x_i^t = \sum_{j \in \mathcal{S}} a_{ij}x_j^{t-1} + \epsilon^t \tag{2}$$

Ordinary least square (OLS) linear regression:
Optimization technique for the MVAR process to estimate the linear interaction strengths.

for $2 \leq t \leq T$. When T is large and \mathcal{S} contains all nodes, the estimated coefficients a_{ij} converge toward A_{ij} . With abuse of notation, we define the residual ϵ as the standard deviation of the ϵ^t for the ordinary least square (OLS) regression in Equation 2, standard deviation of error residuals

$$\epsilon(x_i^{2 \leq t \leq T} | x_i^{1 \leq t \leq T-1}) = \sqrt{\sum_t (\epsilon^t)^2}, \tag{3}$$

with a notation similar to conditional probabilities; the superscript t indicates the considered time range and the subscripts indicate the nodes involved. To detect the existence of connection $j \rightarrow i$ in a network, two types of Granger causality analysis exist: “unconditional” and “conditional” (Geweke, 1982, 1984); they consider the comparisons of the following residuals:

$$\begin{aligned} \text{GRu}(x_j \rightarrow x_i) &= \ln \left[\frac{\epsilon(x_i^{2 \leq t \leq T} | x_i^{1 \leq t \leq T-1})}{\epsilon(x_i^{2 \leq t \leq T} | x_{ij}^{1 \leq t \leq T-1})} \right]; \\ \text{GRc}(x_j \rightarrow x_i) &= \ln \left[\frac{\epsilon(x_i^{2 \leq t \leq T} | x_{1, \dots, j-1, j+1, \dots, N}^{1 \leq t \leq T-1})}{\epsilon(x_i^{2 \leq t \leq T} | x_{1, \dots, N}^{1 \leq t \leq T-1})} \right]. \end{aligned} \tag{4}$$

For both GRu and GRc, which have a univariate target node x_i , the usual parametric test for significance relies on the F statistic, which performs better for a small number of samples (Barnett & Seth, 2014). The null hypothesis of no interaction for $\text{GRu}(x_j \rightarrow x_i)$ corresponds to $m = T$, $p = 1$, $n_x = 1$, and $n_y = 2$ using the notation in Barnett and Seth (2014):

$$\frac{\epsilon(x_i^{2 \leq t \leq T} | x_i^{1 \leq t \leq T-1}) - \epsilon(x_i^{2 \leq t \leq T} | x_{ij}^{1 \leq t \leq T-1})}{\epsilon(x_i^{2 \leq t \leq T} | x_{ij}^{1 \leq t \leq T-1})} = [\exp(\text{GRu}_{ij}) - 1] > \frac{\Phi(\alpha, 1, T-3)}{T-3} \tag{5}$$

with α the desired sensitivity and ϕ the inverse survival function of the F distribution (Scientific Python Library, n.d.). The equivalent for GRc corresponds to $n_y = N$, yielding

$$\frac{\epsilon(x_i^{2 \leq t \leq T} | x_{1, \dots, N}^{1 \leq t \leq T-1}) - \epsilon(x_i^{2 \leq t \leq T} | x_{1, \dots, j-1, j+1, \dots, N}^{1 \leq t \leq T-1})}{\epsilon(x_i^{2 \leq t \leq T} | x_{1, \dots, j-1, j+1, \dots, N}^{1 \leq t \leq T-1})} > \frac{\phi(\alpha, 1, T - N - 1)}{T - N - 1}. \quad (6)$$

Circular shift of time series:
The new start is set to a given position and remaining early entries are sequentially moved after the end of the original series.

We also use nonparametric tests for GRc by performing a circular shift (see details in the section below, Generation of Surrogate Time Series) either on the target node for each connection (Faes et al., 2014) or independently on the time series of all nodes (in order to save time in estimating the full network's connectivity by shuffling somehow all targets simultaneously). Both cases provide a null distribution for the log ratio, with which the actual estimated log ratio can be compared.

Multivariate Autoregressive Estimation

To detect the existence of connections $A_{ij} > 0$, another possibility is to estimate the coefficients themselves, which can be done using the covariances of the observed activity variables x^t (Lütkepohl, 2005):

$$\hat{Q}_{ij}^\tau = \frac{1}{T - \tau_{\max} - 1} \sum_{1 \leq t \leq T - \tau_{\max}} (x_i^{t+\tau} - \bar{x}_i)(x_j^t - \bar{x}_j), \quad (7)$$

where T denotes the number of successive samples indexed by t , $\tau \in \{0, 1\}$ is the time shift (here $\tau_{\max} = 1$), and the observed mean activity for each node is $\bar{x}_i = \frac{1}{T} \sum_t x_i^t$. The Yule-Walker equation gives a consistency equation for the theoretical covariance matrices (Q^τ) in terms of the connectivity A in the dynamics described by Equation 1:

$$Q^1 = A Q^0. \quad (8)$$

The estimation of network connections relies on evaluating A from Equation 8 for the empirical covariance matrices defined as Equation 7 and calculated for a given time series:

$$a = \hat{Q}^1 (\hat{Q}^0)^{-1}. \quad (9)$$

Note that this OLS estimate corresponds to the linear regression related to $\epsilon(x_{1, \dots, N}^{2 \leq t \leq T} | x_{1, \dots, N}^{1 \leq t \leq T-1})$ and also to the linear model with maximum likelihood under the assumption that the observed process is Gaussian.

MVAR of Order 2

Equation 1 can be extended to the case where the activity vector x^t is determined by the two previous time steps:

$$x^t = A^1 x^{t-1} + A^2 x^{t-2} + \zeta^t. \quad (10)$$

For the second order, we use $\tau_{\max} = 2$ in Equation 7 and the estimation of A^1 and A^2 via the Yule-Walker equation is given by (Lütkepohl, 2005, p. 86)

$$\tilde{a} = \tilde{Q}^1 (\tilde{Q}^0)^{-1}, \quad (11)$$

with the block matrices

$$\begin{aligned} \tilde{a} &= \begin{pmatrix} a^1 & a^2 \end{pmatrix}, \\ \tilde{Q}^0 &= \begin{pmatrix} \hat{Q}^0 & \hat{Q}^1 \\ (\hat{Q}^1)^\dagger & \hat{Q}^0 \end{pmatrix}, \\ \tilde{Q}^1 &= \begin{pmatrix} \hat{Q}^1 & \hat{Q}^2 \end{pmatrix}. \end{aligned} \tag{12}$$

The coefficients of A^1 and A^2 can thus be estimated using a matrix multiplication and an inversion involving the covariances, as with the first-order case in Equation 9.

Generation of Surrogate Time Series

In this paper, we consider circular shifts (CS), random permutations (RP), and phase randomization (PR) to shuffle the time points of the observed time series. From the original x_i^t with $1 \leq t \leq T$,

Random permutation of time series: Shuffling of the time labels in time series to destroy their temporal arrangement when generating surrogates for nonparametric test.

- CS draws a random integer $t_0 \in \{1, \dots, T\}$ and returns $(x_i^{t_0}, \dots, x_i^T, x_i^1, \dots, x_i^{t_0-1})$;
- RP draws a random permutation σ of $\{1, \dots, T\}$ such that each integer appears once (and only once) and returns $x_i^{\sigma(t)}$;
- PR calculates the discrete Fourier transform $\mathcal{F}(x_i^t)$ of the original x_i^t , then multiplies each of the T coefficients of $\mathcal{F}(x_i^t)$ by $\exp(2\pi i \phi^t)$ with ϕ^t randomly chosen in $[0, 2\pi]$, and performs the inverse transform.

Importantly, these operations are applied to each time series independently of the others.

In addition, we consider the replacement of all time series in the network by T zero-mean and normally distributed variables with a standard deviation equal to the average standard deviation of x_i^t along the time axis, over all nodes. We refer to these surrogates as STD.

Experimental Setup and Processing of Electrode Measurements to Extract MUAe Activity

All procedures were carried out in accordance with the European Communities Council Directive RL 2010/63/EC, the U.S. National Institutes of Health Guidelines for the Care and Use of Animals for Experimental Procedures, and the U.K. Animals Scientific Procedures Act. Two male macaque monkeys (5–14 years of age) were used in the experiment; only the data for the first one are used here. A surgical operation was performed under sterile conditions, in which a custom-made head post (Peek, Tecapeek) was embedded into a dental acrylic head stage. Details of surgical procedures and postoperative care have been published previously (Thiele, Delicato, Roberts, & Gieselmann, 2006). During the surgery microelectrode chronic Utah arrays (5×5 grids), attached to a CerePort base (Blackrock Microsystems) were implanted into V1. Electrodes were 1 mm in length in line with procedures described in Supèr and Roelfsema (2005). Stimulus presentation was controlled using Cortex software (Laboratory of Neuropsychology, NIMH, <http://dally.nimh.nih.gov/index.html>) on a computer with an Intel Core i3-540 processor. Stimuli were displayed at a viewing distance of 0.54 m, on a 25" Sony Trinitron CRT monitor with a resolution of 1280 by 1024 pixels, yielding a resolution of 31.5 pixels / degree of visual angle (dva). The monitor refresh rate was 85 Hz for monkey 1, and 75 Hz for monkey 2. A gamma correction was used to linearize the monitor output, and the gratings had 50% contrast. Monkeys performed a passive viewing task where they fixated centrally while stationary sinusoidal grating of either horizontal or vertical orientation and 2 cycle per degree spatial frequency were presented in a location that covered all receptive

fields recorded from the 25 electrode tips. Stimuli were presented 500 ms after fixation onset for 150 ms. Raw data were acquired at a sampling frequency of 32556 Hz using a 64-channel Digital Lynx 16SX Data Acquisition System (Neuralynx, Inc.). Following each recording session, the raw data were processed offline using commercial software (Neuralynx, Inc.). Signals were extracted using Cheetah 5 Data Acquisition Software, with bandpass filtering set to allow for spike extraction (600-9000 Hz) and saved at 16-bit resolution.

In the present study, we focus on the period starting 200 ms before and finishing 200 ms after the stimulus onset, for 4 conditions (vertical gradings with pre/post cue in the receptor/opposite field) that will not be compared in details. The electrode recordings is firstly down-sampled from 32,556 Hz to 1,000 Hz. A high-pass filter above 400 Hz is then applied—third-order Butterworth filter at 0.8 of the Nyquist frequency (Scientific Python Library, n.d.)—followed by a smoothing of 4 ms to extract the envelope of the resulting signal, thus retaining the 250 time points of 1,000-ms period surrounding the stimulus onset.

BENCHMARK OF DETECTION PERFORMANCE FOR SYNTHETIC DATA

The workflow of the benchmark for the estimation procedure is schematically represented in Figure 1A. We first consider an MVAR process defined by Equation 1 with given connectivity matrix A and input covariances (obtained by mixing independent Gaussian processes) to generate the activity of the network. From the observed activity over a period of duration T , we estimate the coefficients matrix A using the covariances as described in Equation 9. We also perform the linear regressions of each node activity over the past activity of given subsets of nodes corresponding to the unconditional (GRu) and conditional (GRc) Granger causality analysis, from which we calculate the ratios of residuals in Equation 4. Actually, these estimates correspond to the same OLS regression (top right in Figure 1A) and the difference resides in the spaces where they lie: coefficients versus residuals.

For each method, the prediction power can be measured by the relationship between the estimated values and the original connectivity values, as illustrated in Figure 1B (left). To discriminate between existing and absent connections, one can apply a common threshold for all connections (top thread); by sliding this threshold, we obtain the ROC (receiver-operating characteristic) curve with the rates of false alarms on the x-axis and of true positives on the y-axis. The area under the curve indicates in a single value how well the ranking of estimates performs for the detection of connections with respect to the original connectivity. Alternatively, an individual test can be made for each connection with respect to the network, for example by comparing the estimated value to a null distribution (bottom thread). We then obtain the false-positive and true-positive rates by pooling the results over all connections.

Coefficients from Linear Regression Potentially Predict Better Existing Connections Than Residuals

We start with the comparison between the predictability of coefficients and residuals for MV, GRu, and GRc for all connections in a given network. To do so, we simulate 500 randomly connected networks, which are simulated with different sizes ($N = 50$ to 150 nodes), density, and connectivity weights (uniformly drawn in a randomly chosen range $[w_{\min}, w_{\max}]$). Here inputs are *not* correlated; the ζ_i are independent across node indices in Equation 1. For each network configuration, we evaluate the accuracy for connection detection via the area under the ROC curve (see the upper thread in Figure 1B). Figure 2A displays this ROC-based accuracy as a function of the number of observed time samples (x-axis) represented by violin plots for

ROC curve:
Curve describing the performance of a binary detector when moving its discrimination threshold.

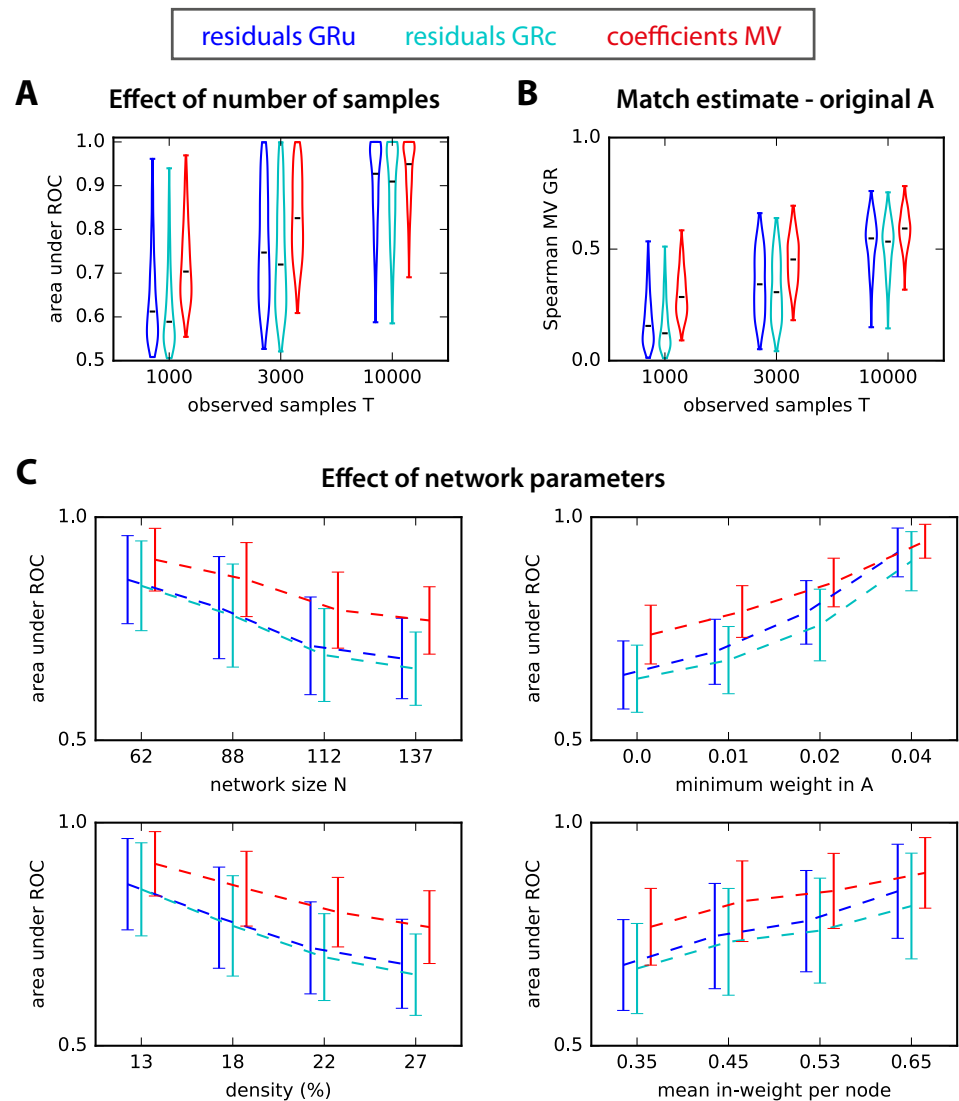


Figure 2. ROC-based prediction power. (A) Area under ROC for estimated A obtained from log ratios of residuals obtained from Granger causality analysis (unconditional for GRu and conditional for GRc) and MVAR. The x-axis indicates three sample size T for the observed network activity. The violin plots correspond to 500 simulated networks of various sizes and connectivity strengths (the horizontal black bar indicates the median). (B) Match of the ranking between GRu, GRc, and MVAR estimates and the original connectivity weights A , as measured by the Spearman correlation coefficient. The plotted values correspond to the 500 networks in A and the x-axis indicates the sample size T . (C) Effect of network parameters on ROC-based performance. Influence of network size N , connectivity density, sum of recurrent connectivity strengths, minimum weight w_{\min} in A , mean noise on the diagonal of Σ , and mean off-diagonal noise in Σ on the ROC-based accuracy in Figure 2A. In each plot, the network configurations have been grouped in quartiles according to the parameter plotted on the x-axis, and the corresponding group mean and standard deviations are indicated; the curves are displaced horizontally to improve legibility.

500 randomly connected networks. When considering many samples (10^4), all methods perform well. However, for smaller sample sets, the MVAR method exhibits superior performance than GRu: as measured by the Mann-Whittney test, $p < 10^{-45}$, $p < 10^{-19}$, and $p < 10^{-5}$ for the three values of observed samples, respectively.

Although error residual ratios are in a different space from the true weights in A , one expects some degree of correlation between them, such that Granger causality analysis effectively detects connections. In Figure 2B, both GRu and GRc estimates have a ranking similar to the original A weights (as measured by the Spearman correlation) for $T = 10,000$ observed time samples, but this weakens dramatically for $T \leq 3,000$. In contrast, the ranking for estimated MVAR coefficients reflects much better the original A for $T \leq 3,000$. In the studied networks, GRu performs slightly better than GRc. As analyzed in previous studies, this can be a consequence of the balance between redundant and synergistic activity exhibited by the simulated network nodes (Stramaglia et al., 2014). To shed light into the effect of the network structure, we next examine how the ROC-based performance in Figure 2A depends on the controlled network parameters. The four panels in Figure 2C display the trends of the values for the 500 networks as a function of the network size N , the network density, the minimum weight in the original network (w_{\min} mentioned above), and the mean sum of incoming weights per node. For illustration purpose, the 500 networks are grouped in quartiles for each parameter. Not surprisingly, the estimation accuracy of all methods decreases as a function of the network size N and density, and increases as a function of the minimum connectivity weight and the mean incoming weight per node. More interestingly, in challenging configurations with small weights, MVAR consistently shows a superior performance by a larger gap compared with Granger causality analyses. These findings support the use of coefficients to robustly detect connections in recurrently connected networks. Note that GRu performs on average slightly better than GRc here: The discrepancy decreases as a function of the network density, which may follow from lower redundancy in the recurrent network (Stramaglia et al., 2014).

A Robust Nonparametric Significance Test for MVAR

We have so far examined the performance of different estimation methods based on the area under the ROC curve, which corresponds to a single threshold for all connections in a network and combines the information about false alarms and true detection over the whole range of estimated values. However, in the context of real data, the decision for the existence of a connection typically relies on comparing the value of the connection estimate with a given statistical threshold. For GRu and GRc, such parametric tests have been developed, for example, based on the F statistics (Barnett & Seth, 2014). Equivalently, it is sufficient to know how the values of the estimates for absent connections are distributed, in order to select a desired rate of false alarms (type 1 error). In this section, we develop a significance test for the estimated MVAR coefficients by providing a null-hypothesis distribution for absent connections.

Our approach relies on the fact that covariances reflect the underlying connectivity. We thus construct the null distribution for estimates by performing a random permutation for each of the observed time samples, which “destroys” the covariance structure apart from the variances on the diagonal of \hat{Q}^0 as illustrated in Figure 3A; other methods will be tested in a later section. From the resulting covariance matrices, we evaluate a surrogate connectivity matrix. The core result underlying our surrogate approach is shown in Figure 3B. The distribution of surrogate estimates (thick black line) is compared against the distribution of existing (red) and absent (blue) connections in a simulated random network model. The surrogate distribution in black provides a good approximation for the distribution of estimates for nonexisting connections in blue.

We consider two options—corresponding to the two threads in Figure 1B—to test the existence of a connection from an MVAR estimate while keeping the false-alarm rate under control.

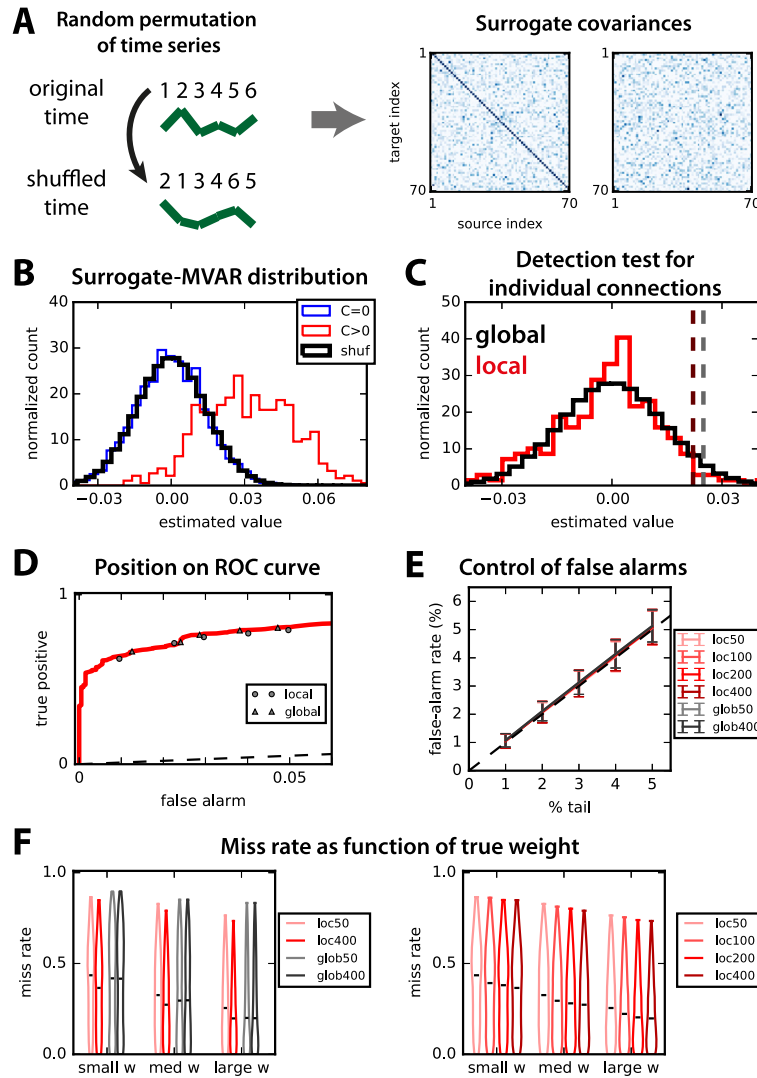


Figure 3. Nonparametric test to assess significance for MVAR coefficients based on random permutations. (A) Schematic illustration of random permutation (numbers indicate time) applied independently to all observed time series (green curves) to generate the surrogate covariances (right panels). (B) Pooled distributions of estimated weights for the existing (in red) and absent (blue) connections. The thick black curve indicates the distribution of connections over 100 surrogates, which closely matches the blue distribution. (C) For a given connection, we compare two methods: for “local” in red, the null distribution corresponds to the matrix elements for the same connection in 200 surrogates; for “global” in black, the null distribution is the pooled distribution for all N^2 elements of the 200 surrogate matrices (same as in B). The dark red and gray dashed lines indicate the detection thresholds corresponding to the 4% tail for those two options. (D) The performance of the two nonparametric methods for the thresholds described in B and C is displayed on the ROC curve for a desired false-alarm rate ranging from 1% to 5%. Triangles indicate the global test and circles the local test. (E) Comparison of the desired (% of the tail of null distribution) and actual rate of false alarms for the local and global tests when varying the the number S of surrogates (see figure in legend). Error bars indicate one standard deviation for 500 random networks; importantly, inputs for these networks have cross-correlation, unlike Figure 2. (F) Influence of the strength of original weight on the detection performance for the 500 random networks and a desired false-alarm rate set to 2% in E. In both panels, lighter colors indicate smaller numbers of surrogates S , in red for the local test and gray for the global test (see legends).

- The *global* test relies on the null distribution corresponding to the black histogram in Figure 3C, which is obtained by grouping together all SN^2 matrix elements of all matrices for $S = 200$ surrogates. From that surrogate distribution, we perform a detection test by setting a threshold corresponding to a percentage of the right tail equal to the desired false-alarm rate (here 2%), as illustrated by the vertical gray dashed line.
- Instead, the *local* test uses for each connection the surrogate distribution of S values, corresponding to the same matrix element in each of the S surrogates. From that distribution in red in Figure 3C, the detection threshold is defined similarly (vertical dark red dashed line).

The rationale behind these two choices lies in the trade-off between taking into account spatial heterogeneity in the network and gaining larger sample size, as illustrated by the distinct thresholds in Figure 3C. Note also that the F statistical test for Granger causality analysis corresponds to a global threshold on the log ratio values. When varying the desired false-alarm rate, the two tests perform well, as illustrated in Figure 3D by their location close to the ROC curve (circles and triangles for local and global, respectively).

To quantify the small variability observed in Figure 3D over the randomness of network configurations, we simulate 500 randomly connected networks with the same parameters as in Figure 2, except for the size $50 \leq N \leq 90$ and the presence of input cross-correlations. Note that, from Figure 2, the chosen size N corresponds to a situation where Granger causality analysis performs relatively well as compared with MVAR. The control of the false-alarm rate is displayed in Figure 3E for both local and global tests with various numbers S of surrogates. The control of false-alarm rates is close to perfect across various values for all S and both tests (local and global), demonstrating the robustness of the proposed method for randomly connected networks. Next, we fix the desired false-alarm rate to 2% and evaluate the miss rate (true negatives) of both methods depending on the actual weight strength: In Figure 3F, connections are grouped in terciles for each network configuration. Interestingly, the local test improves with the number S of surrogates (right panel), whereas the global test exhibits a constant performance for all S (left panel). Note that the advantage of the local test over the global test particularly concerns connections with small weights, which are difficult to detect, in line with Figure 2C (see influence of the minimum original weight).

Because GRu does not take all network nodes into account, the presence of spatially correlated noise (indicated by the purple dashed arrows in Figure 1A) dramatically affects the false-alarm rate when using the parametric significance F test (Barnett & Seth, 2014), as shown in Figure 4A by the dark blue dashed curve. This is solved by the “complete” linear regression in GRc, achieving a quasi perfect control irrespective of the input correlation level for both the parametric and two nonparametric tests (cyan, green, and blue-green dashed curves, respectively), as our nonparametric tests do (red and gray; recall also Figure 3E). We consider two nonparametric tests for GRc: “T” stands for target, where the null distribution of a connection is obtained by shuffling only the target, and “F” stands for full, where we shuffle all time series simultaneously as in our coefficient-based tests. Both perform equally in terms of false alarms.

The main result of the paper is described in Figure 4B, where the dashed line corresponds to the miss rate for parametric GRc: Our nonparametric method exhibits a better than miss rate—that is, decrease—for both local and global tests (in red and gray, respectively) on average over the same 500 random networks as in Figure 4A. For $S \geq 200$, the local test even becomes better in all cases. Note that the small miss-rate improvements of about 7% actually correspond

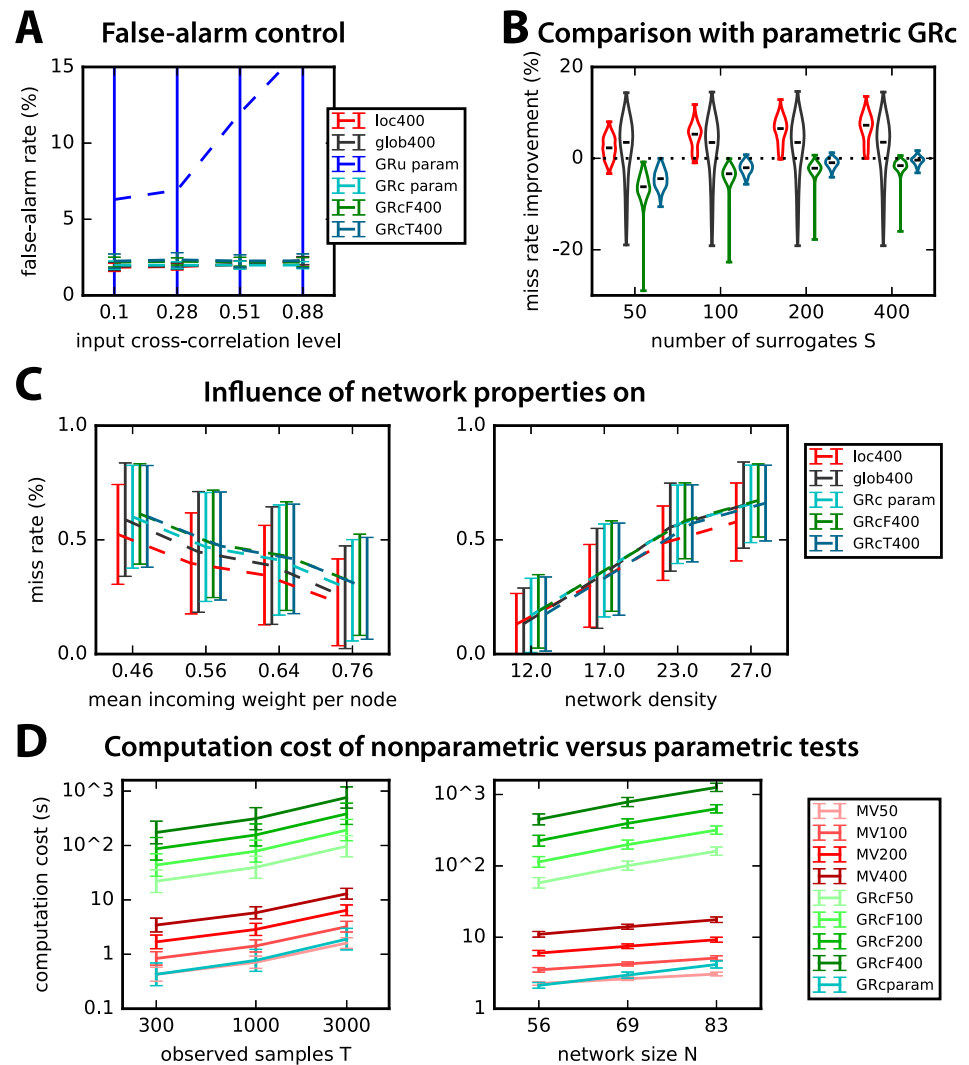


Figure 4. Comparison of our coefficient-based method with Granger causality analysis. (A) Comparison of the parametric tests for GRu (blue curve) and GRc (cyan) with the nonparametric methods for GRc (green for GRcF and blue-green for GRcT; see the text for details) and MVAR (red for local test and gray for global). The x-axis indicates the strength of input correlations (i.e., pink noise) in the simulated network. The desired false-alarm rate is set to 2% as in Figure 3F and the number of observed time samples is $T = 3,000$. Error bars indicate one standard deviation over the 500 random networks as in Figure 3E. (B) Comparison of the miss rate improvement (decrease) with respect to parametric GRc for the 500 networks in A as a function of the number S of surrogates (x-axis). Red indicates the local test, gray the global test, green the full-network nonparametric GRc, and blue-green the target-only nonparametric GRc. (C) Details of the performance of the five methods in B as a function of the mean incoming weight per node (left) and the network density (right). The plots for the miss rate are similar to those for the ROC-based prediction power in Figure 2C. (D) Comparison of the computational cost for the surrogate-based method and parametric tests as a function of the number T of observed samples (left) and network size (right). Only GRcF is shown, as GRcT takes a much longer time in the unoptimized version that we use.

to more than 50 existing connections per network here. In contrast, both nonparametric tests for GRc perform worse than the parametric test here, with the target-shuffling surrogate converging faster to the nonparametric GRc. Figure 4C displays the trends of the performance of all five tests in Figure 4B as a function of two network properties: the mean incoming weight

per node (left) and the density (right). The main result here is that the local test performs better especially in difficult configurations with small weights and dense connectivity.

From Figures 3F and 4B–C, we conclude that the local test is preferable to the global test provided $S \geq 200$ surrogates are generated. However, the computational cost increases linearly with S , as illustrated in Figure 4D by the red curves. Note that the parametric GRc (in cyan) takes the same time to calculate as $S = 50$ surrogates. However, our nonparametric method scales better than parametric GRc when the network size increases. As a comparison, the full-network nonparametric test for GRc takes a longer time to compute, but further optimization of the calculations could be made that were not incorporated here.

Comparison of Generation Methods for Surrogates for Nonparametric MVAR

The fact that the OLS MVAR estimates can be obtained via the two covariance matrices (with and without time shift; see Figure 1A) hints at possible methods to generate surrogate by destroying the structure in these covariances. Methods to generate surrogate time series have been widely used in the past: circular shifts of the time series (Faes et al., 2014), random permutation (Winkler et al., 2014), and phase randomization (Schreiber & Schmitz, 1996) to generate a null distribution for the ratios in Equation 4; they are referred to here as CS, RP, and PR, respectively. We thus consider these three methods (cf. box in Figure 5), as well as surrogate time series that only preserve the mean standard deviation averaged over the network (STD), so as to test to what extent it is important to preserve the spatial heterogeneity of the nodes' activity. See Methods for details about the calculations.

The control of false alarms for local tests in Figure 5A and B is better for CS and RP, whereas the detection of true connections is similar for the four methods over 500 random networks of size $N = 70$. However, CS fails to detect self-connections (Figure 5C). The reason is that, because CS surrogates preserve the autocovariances in the time-shifted covariance, they fail to build a proper null distribution for self-connections. The influence of the number of samples used in the estimation is similar for all methods, as illustrated in Figure 5D. The comparison with STD (purple), which averages the covariance statistics over the whole network, suggests that the local test makes a good use of the heterogeneous information across nodes. As a conclusion, we retain RP as the best option.

Influence of Network Topology

In this part, we test and compare the robustness of global and local surrogate-based detection tests to specific connections and topological configurations. Here, $T = 3,000$ observed samples and we compare the local and global tests with $S = 400$ surrogates for 500 networks of each type. In all cases, the simulated networks have the same size $N = 70$, but they vary in connectivity density, distribution of recurrent weights and level of input cross-correlation. We compare the miss rate for unidirectional, reciprocal, and self-connections in the random networks examined until now (and a desired 2% of false alarms). Figure 6A shows that the miss rate is similar in unidirectional and reciprocal connections with the local test, which performs slightly better than the global test (as in Figure 3F).

Now we consider more elaborate network topologies than the random connectivity (Erdős-Rényi) considered so far, namely modular and hierarchical networks. In Figure 6B, we simulate 500 modular networks with two groups (green and blue) linked by hubs (red, about 5 to 15% of the nodes). Interestingly, intragroup and hub-group connections have a similar miss rate with

Modular and hierarchical network topology:
Nonrandom connectivity giving heterogeneous statistics (e.g., number of connections) across nodes.

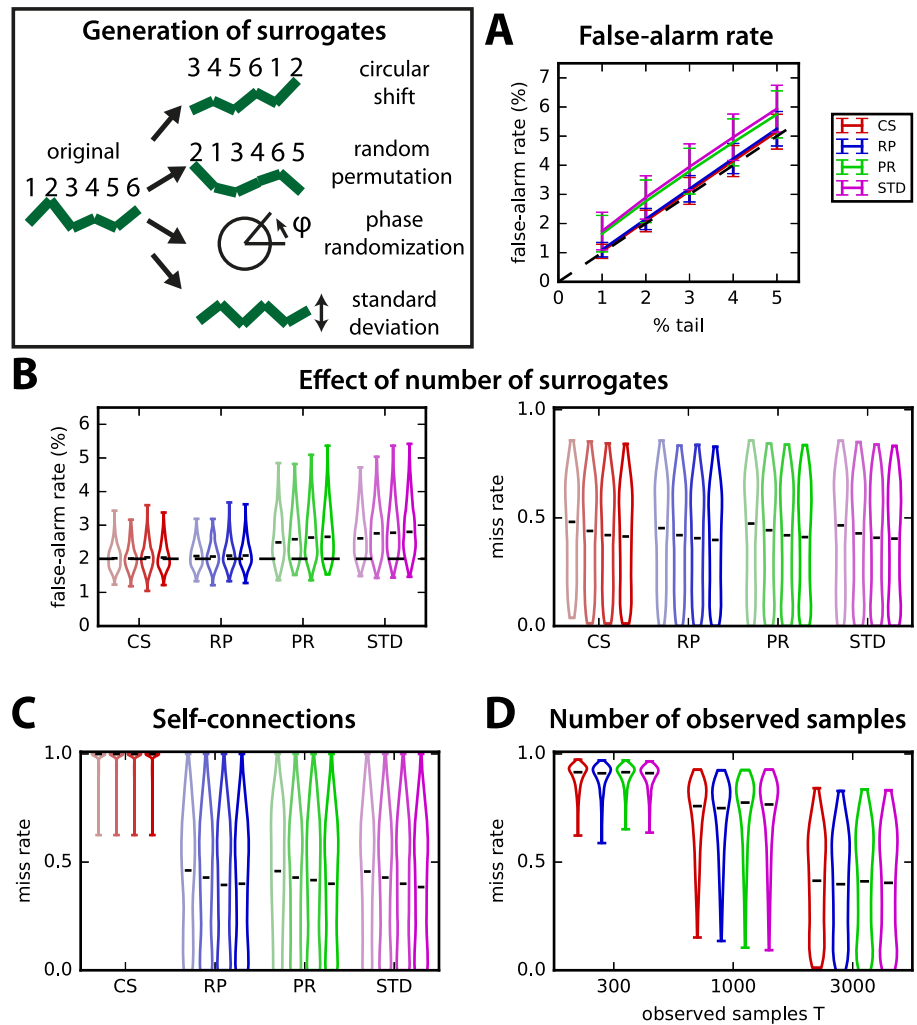


Figure 5. Comparison of the local test for four surrogate generation methods. Surrogates are generated by independently performing for each original time series (1) random permutations, (2) circular shifts, (3) phase randomization, and (4) replacing the original by a new random time series with the mean standard deviation averaged over all of the original time series in the network. (A) Comparison of the control of the false-alarm rate for various thresholds on the tail of the distributions of 400 surrogates (% indicated on the x-axis). The error bars correspond to the variability over 500 random networks similar to Figure 3 with $T = 3,000$ observed time samples and the local test. (B) Influence of the number S of surrogates on the detection performance for the four surrogate methods (x-axis). The violin plots indicate the distribution of false-alarm rates (left panel) and miss rates (right) for the 500 networks in A with a desired false-alarm rate set to 2% (dashed line in the left panel). Lighter to darker colors correspond to 50, 100, 200, and 400 surrogates, respectively. (C) Same as the miss rate in B, but only for self-connections. (D) Influence of the number T of observed time samples on the miss rate for $S = 400$ surrogates.

regard to using local and global surrogates. In Figure 6C, we simulate hierarchical networks of three layers, for which connections either link the center and an intermediate node, or link an intermediate node and a leaf, or are self-connections. This network type is much sparser than the two types in A and B, yielding a quasi perfect detection performance for all types of connections (miss rate < 0.1 in Figure 6C). In all cases, the local test performs better than the global test. However, the control of false-alarm rate is similar for both tests with all topologies, as can be seen in Figure 6D.

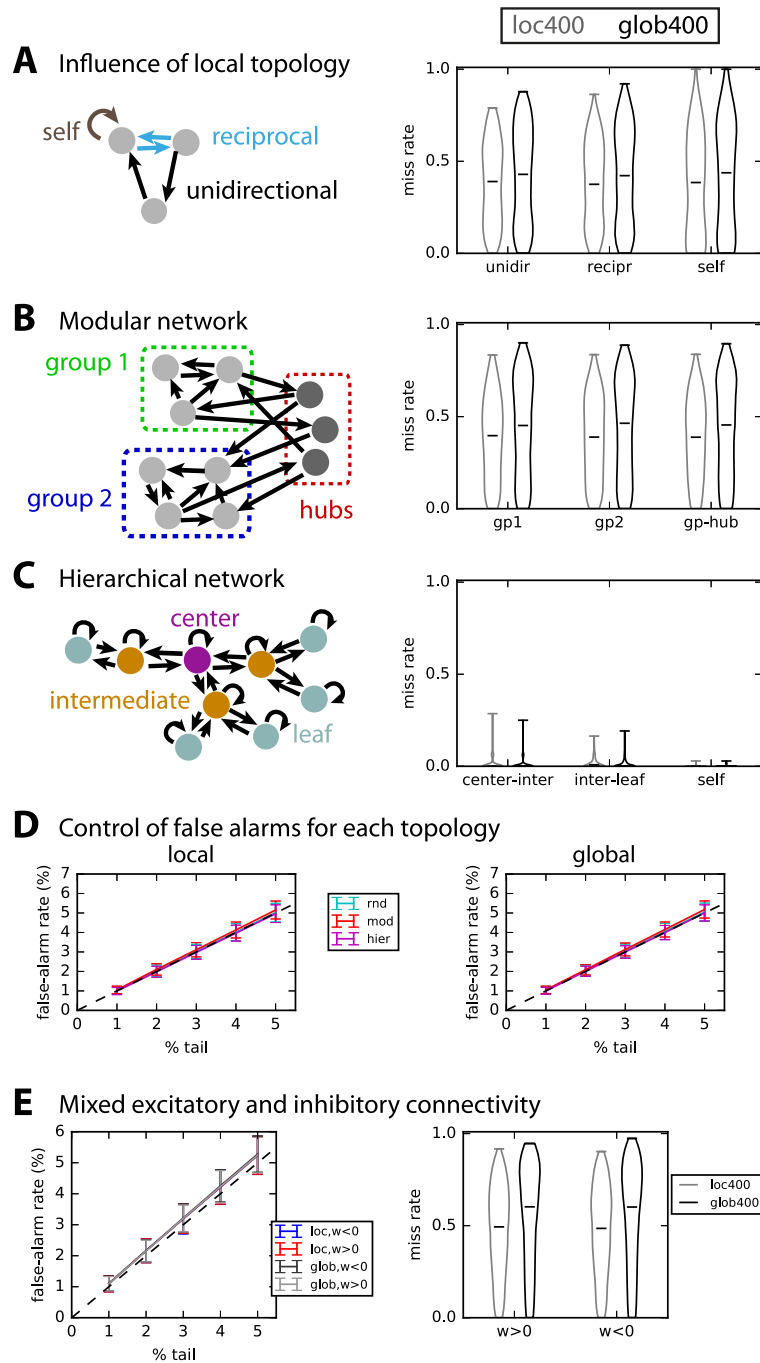


Figure 6. Robustness to nontrivial network topology. (A) Detection performance for unidirectional, reciprocal, and self-connections in 500 of the randomly connected networks used so far in Figure 3. (B) Detection performance for modular topology schematically represented in the left: each of the 500 networks composed of two groups connected by hubs. The connections are separated depending on whether the connect group nodes or hubs, as indicated by the diagram on the left. (C) Similar to B with a hierarchical topology, where connections are grouped in three subsets: from center to intermediate nodes; from intermediate nodes to leaves; self-connections. Note that the density for all 500 networks is very low. (D) Control of false-alarm rate for the local (left) and global (right) significance tests and the three network topologies; the plot is similar to Figure 3E. (E) Control of false-alarm rate and miss rate for networks with both excitatory and inhibitory connections.

Finally, we consider a network with both excitatory and inhibitory connections (with an inhibitory ratio equal to 5 to 50% of all) and perform the test by defining a threshold on both tails of the null distributions. As can be seen in Figure 6E, the positive/negative nature of the connection weights affects neither the false-alarm nor the miss rate. However, the performance is poorer than with excitatory connections only.

We conclude that, in those networks with spatial heterogeneity as with randomly connected networks, the local test with an individual null distribution per connection performs better than the global test. Recall that an improvement of the miss rate by 1% in a network with a density of 20% actually corresponds to $N^2 \cdot 0.2 / 100 \simeq 10$ existing connections here, so the plotted improvements concern about 50 connections.

Applicability to Second-Order MVAR Process

As explained in Methods, an MVAR process whose state depends on the two previous time steps can be estimated with the covariances with time shifts $\tau = 0, 1$, and 2; see Equations 11 and 12 for details. Here we simply focus on random connectivity for the two corresponding matrices A^1 and A^2 , with size N that is randomly drawn between 30 and 80; we construct A^1 and A^2 such that a connection $j \rightarrow i$ cannot be in both matrices, but at most in one. The existing connections are detected with the nonparametric local test relying on RP surrogates for each matrix separately, as a proof of concept. The control of false alarms in Figure 7A and the overall detection performance in Figure 7B suggest that our surrogate method can be extended satisfactorily to higher-order MVAR processes. Note that the improvement by generating more

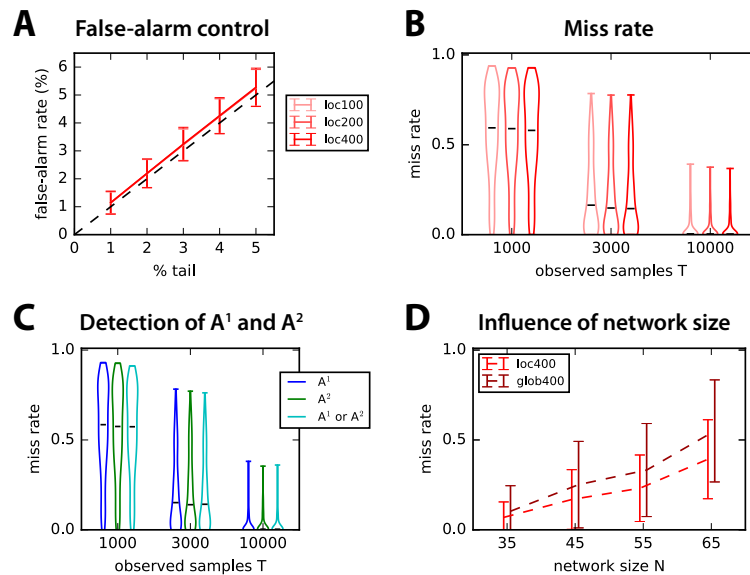


Figure 7. Connectivity detection for second-order MVAR process. (A) Control of false-alarm rate for the local test with $S = 100, 200$, and 400 in both connectivity matrices A^1 and A^2 , corresponding to each time step. Error bars correspond to the variability over 500 network configurations with random connectivity and $T = 3,000$ observed samples. (B) Influence of the number T of observed samples (x-axis) on the miss rate for the 500 networks in A. Lighter to darker red indicates the number of surrogates S . (C) Details of the detection performance for A^1 and A^2 separately, as well as connections in either A^1 or A^2 . The number of observed samples is indicated on the x-axis as in B. (D) Influence of the network size N on the detection performance in C for the local and global tests with $S = 400$ surrogates.

Multiunit activity:
High-frequency signal from simultaneous extracellular recordings (e.g., electrode array), presumably related to the spiking neuronal activity.

surrogates is rather weak here. Importantly, there is no difference between the detection in A^1 and A^2 , as demonstrated in Figure 7C. Last, the network size worsens the miss rate in Figure 7D, which affects more dramatically the global test as compared with the local test.

APPLICATION TO EXPERIMENTAL DATA

Multiunit Activity Data Obtained from Utah Electrode Array in Monkey

Now we consider data recorded from a monkey performing a visual task, where the stimulus corresponds to vertical gratings covering all recorded V1 receptive fields from the Utah arrays (see Methods for details). We aim to provide a proof of concept for the connectivity analysis for this type of data, so as to complement the more classical analysis based on the activity of individual channels; therefore, we do not focus on comparing the four stimulus conditions with each other.

The multiunit activity envelope (MUAe) is obtained as described in Methods. In Figure 8A, the resulting MUAe is represented for two out of the 26 channels (red and purple) for two trials in the top and middle panels, 400 ms before and 600 ms after the stimulus onset. The typical analysis of MUAe activity consists of averaging over 200 trials, which exhibits a peak immediately after the stimulus for the two channels in the bottom panel. Among the 26 channels,

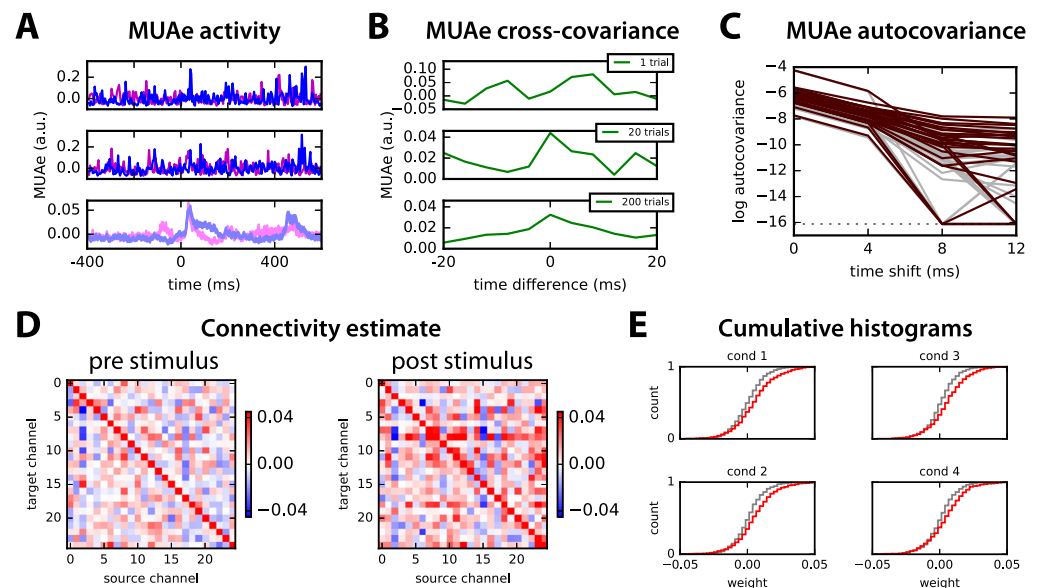


Figure 8. Application to multiunit activity (MUAe) data. (A) Example of two trials (top and middle panels) of multiunit activity envelope (MUAe) for two channels of recordings using Utah electrode array in the primary visual cortex of a monkey (in arbitrary units; see text for further details). The bottom panel represents the average over 200 trials (with standard-error mean for the thickness of the curve). The stimulus is presented at time point 100 (actually 400 ms, since the smoothing corresponds to a smoothing window of 4 ms). (B) Example of cross-covariance between the two channels in A averaged over 1, 20, and 200 trials. (C) Autocovariance profiles of MUAe signals for all 25 channels and time shifts up to 12 ms averaged over 200 trials plotted with a log y-axis: comparison of signals before (gray) and after (red) the stimulus presentation. (D) MVAR estimates of the connectivity between the 25 channels for the MUAe activity 200 ms before and after stimulus presentation (i.e., 50 time points each), averaged over 200 trials. The scaling has been optimized to enhance the legibility of off-diagonal elements. (E) Comparison of the cumulative distribution of connectivity weights (off-diagonal elements in D) for the four conditions. Gray and red indicate before and after the stimulus, respectively.

about a third show a large increase in activity after the stimulus onset as compared with before (namely, a poststimulus mean activity larger by more than three standard deviations compared with the prestimulus activity); almost all channels show a moderate increase of one standard deviation. One channel is discarded for a much larger activity (by 5 times) than all others.

To further investigate the temporal information conveyed by MUAe jointly for pairs of channels, we calculate the pairwise covariances between them, after centering the MUAe activity individually for each trial. Figure 8B shows the stabilization of the cross-covariance between the two channels in Figure 8A from a single trial to averages over 20 and 200 trials. Note the asymmetry with respect to time difference: This information is extracted by the network model to estimate the interactions between the neuronal populations recorded by the channels. Then we verify that the model can be applied to these data, by examining the MUAe autocovariances in Figure 8C, which exhibit a profile corresponding to an exponential decay up to two time shifts (i.e., 8 ms for the downsampling every 4 ms), that is, a straight line in the log plot. This suits an autoregressive model with large positive values on the diagonal of the connectivity matrix A .

Both connectivity matrices for the 25 channels estimated using the MVAR method before and after the stimulus are illustrated in Figure 8D for condition 1: we find larger off-diagonal values for the period after the stimulus than before. This is actually true for all conditions, as indicated by the more spread distributions in red as compared with gray in Figure 8E. The channels appear to be coordinated at the considered time scale of 4 ms, and their collective interaction scheme is affected by the stimulus presentation.

Significance Test for Real Data: Interactions Related to Stimulus Presentation

We then use the local and global tests based on 1,000 surrogates (with random permutation) to retain only significant interactions from the estimates in Figure 8D: this leaves a few interactions for the prestimulus period in Figure 9A (left panel), 8 out of 650, which is of the order of the desired false-alarm rate set to 1% (namely, the extreme 0.5% of each tail). In contrast, many more poststimulus interactions survive the significance tests in the right panel: almost all these interactions are unidirectional. The counterpart for circular shift for Figure 9B involves 24 interactions in common with Figure 9A. On average over the four conditions, 22 poststimulus interactions are common between the two shuffling methods, to be compared with 7 for the prestimulus period (both with a standard deviation of 4); this corresponds to 3.5% of all possible interactions. Almost all detected interactions are unidirectional, as illustrated in Figure 9C for both local and global tests for the poststimulus period. Varying the threshold on the tail of the null distributions, we see that the number of detected interactions is close to the desired false-alarm rate for the prestimulus period in Figure 9D (dark red and black curves, respectively). In contrast, poststimulus interactions are many more for both local and global tests (light red and gray). The global test detects fewer interactions than the local test, indicating the necessity to take into account the disparities across channels. Around 57% of poststimulus interactions detected by the global test (largest values in absolute value) are found by the local test.

Finally, we check the relationship between the strengths of significant interactions—in absolute value—and the increase of average MUAe observed in Figure 8A (lower panel). In Figure 9E, the plotted dots correspond to the pre-post change in the sum of incoming (left panel) and outgoing (right panel) significant interactions for each node. The summed interaction values positively correlate with the MUAe difference (post minus pre) only for the incoming interactions: $p = 0.03$ with a coefficient of 0.21. In contrast, outgoing interactions

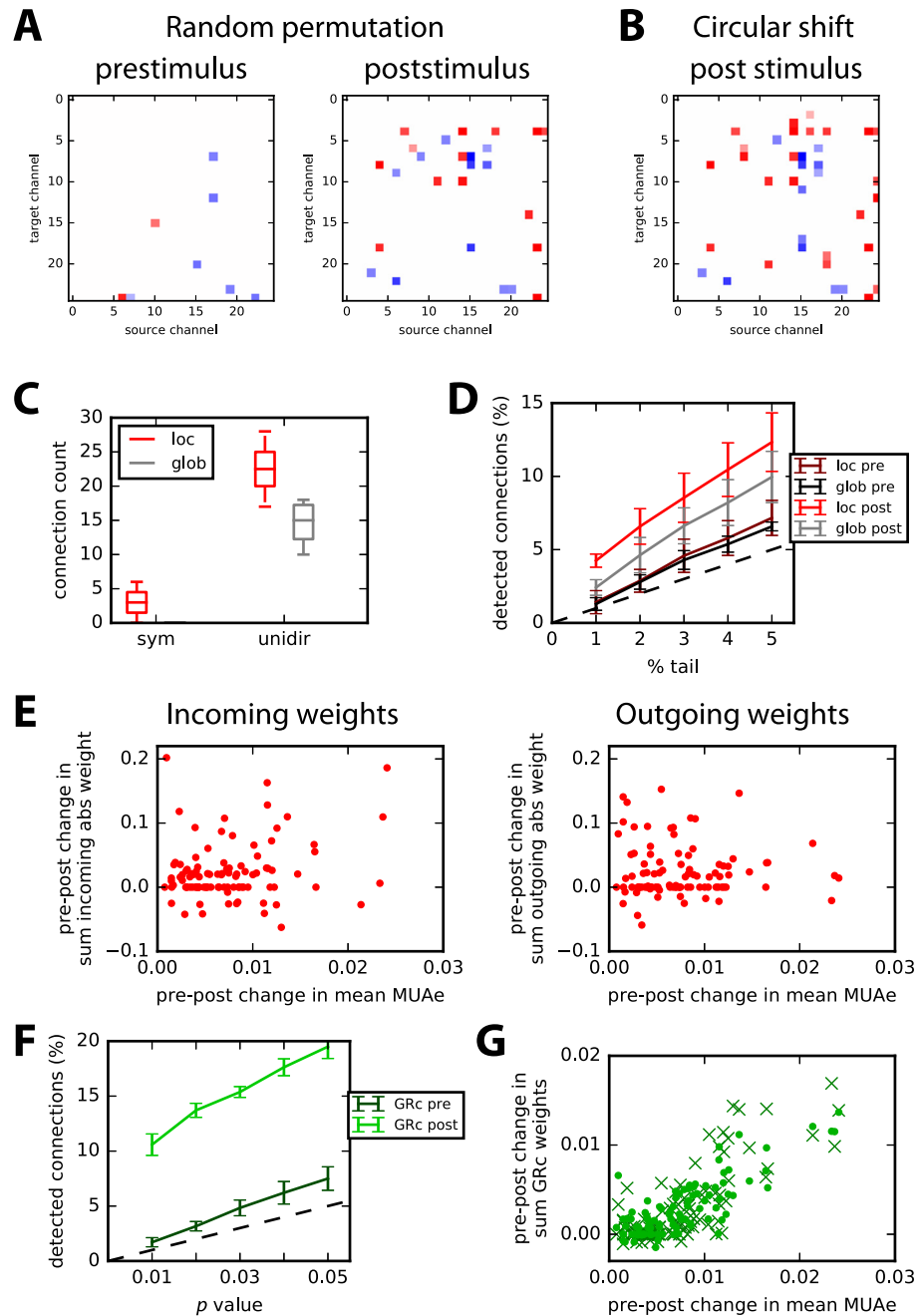


Figure 9. Detection of significant interactions. (A) Examples of significant interactions with the RP surrogate method; left and right panels correspond to pre- and poststimulus periods, respectively. The p value corresponds to the upper and lower 0.5% tails of 1,000 surrogates (local test). Many more interactions are found for post- than prestimulus period. (B) Same as A for the CS surrogate method and poststimulus period. (C) Comparison of number of asymmetric interactions versus symmetric interactions for the local (red) and global (gray) tests over the four conditions. (D) Ratios of detected interactions for pre- and poststimulus periods with the desired false-alarm rate equal to 1% to 5% corresponding to both local and global tests. (E) Change between pre- and poststimulus periods of the sum of incoming (left) and outgoing (right) significant weights—in absolute value—plotted against the change in the change in mean MUAe. Each dot represents a channel, and all four conditions are grouped here. (F) Similar plot to D for parametric GRC. (G) Similar plot to E with sums of GRC values for each node over its incoming (dots) and outgoing (crosses) connections. Only significant interactions passing the parametric test with p value of 0.01 in F are retained here.

exhibit a nonsignificant negative correlation ($p \gg 0.1$). This suggests a stimulus-driven gating of the effective gain for incoming anatomical connections to recorded cell populations. The application of our method thus unravels stimulus-driven directed interactions and cannot be merely explained by an increase of single-channel MUAe activity.

In comparison, similar detection with parametric GRc testing gives more interactions for the poststimulus period in Figure 9F (bright green), twice as much as MVAR for a p value of 0.01 (corresponding to 1% in Figure 9D). Moreover, the distributions of MVAR coefficients in Figure 9E and the corresponding ones for GRc estimated values have similar KS distance when comparing—for each condition—the pre- and post-periods (mean of 0.17 with a standard deviation of 0.01 over the four conditions). This means that GRc values collectively discriminate between the two periods as well as the estimated MVAR coefficients. However, the pre-post changes in incoming and outgoing GRc values strongly correlate with the change in mean MUAe ($p < 10^{-20}$ for both incoming and outgoing connections); note that the estimated connectivity is not symmetric, though. This contrasts with the two plots in Figure 9E and suggests that the two methods may capture distinct effects at work in the network of neuronal populations. Note that the nonparametric method for GRc did not work for the experimental data here, failing to detect more interactions than the expected false-alarm rate.

DISCUSSION

Nonparametric MVAR-Based Detection of Linear Feedback in Recurrent Networks

This paper proposed a nonparametric method to detect pairwise feedback connections in biological networks with possibly strong and/or dense recurrent feedback. We examined the benefit of detecting directional connections in MVAR-like models estimated using the OLS autoregressive coefficients instead of the error residual ratios (Figure 1). To our understanding, the good performance of the presented method has three reasons. First, the ROC-based prediction power in Figure 2, which relies on the estimated ranking of connections in the network (i.e., from small to strong weights), is more robust for the regression coefficients than residual log ratios for recurrent networks with relatively large density (0.1 – 0.3%); these networks overall imply many redundancy and convergence patterns of connections (M. Ding et al., 2006; Stramaglia et al., 2014). Second, practical coefficient-based connectivity detection performed using nonparametric significance tests based on time series randomization (red distribution in Figure 4B) yields better results than conditional Granger causality ratio test in the time domain, either with the standard parametric F test (Barnett & Seth, 2014, dashed line) or with nonparametric testing (green and blue-green distributions). Finally, the use of connection-specific significance testing achieves higher accuracy than a network-pooled alternative, especially when asymptotic assumptions do not hold (e.g., small number of time samples), as illustrated by the local nonparametric test in Figures 3F and 4B (red versus dark gray). Together, our results highlight the need for testing strategies that capture the heterogeneity of sufficiently large networks to detect individual connections. Further note that assessing the connectivity via the regression coefficients space brings an additional advantage for network studies: The estimated connection weights can be interpreted and compared across the whole network, for example using graph theory (Sporns, 2013).

Our approach for generating surrogate distributions can be encompassed in the family of constrained randomization methods (Schreiber, 1998; Schreiber & Schmitz, 1996). Here we have shown that random permutation provides a good estimation of all types of connections (Figure 5) in false-alarm and miss rates. Comparatively, the circular shift method performs

as well except for self-connections that are not detected at all; this also holds for nonrandom topologies (results not shown). Hence, preserving the autocovariance structure in the generation of surrogates does not provide a substantial advantage here (Figure 5B–C). Both methods show a good control for the false-alarm rate in comparison to phase randomization (Schreiber & Schmitz, 1996) and a control Gaussian approximation over the whole network (STD), which lead to an excess of about 1% of false alarms (i.e., ~ 50 connections for a network of 70 nodes). These results show the importance of choosing a surrogate method adapted to the detection problem. For distinct dynamics governing the nodal activity such as nonlinearities, conclusions may differ and further research along these lines is necessary.

As mentioned earlier, the use of an individual null distribution for each connection (local test) gives better results for the miss rate (by a few percentage) than lumping together all matrix elements of all surrogates (global test), provided sufficiently many surrogates are generated. For the size of networks considered here, computation time is not an issue (Figure 4D) and our results support the choice of the local test over the global test to attain between accuracy in the true-positive detection. This may be especially true for specific topologies or networks with both excitatory and inhibitory connections; see Figure 6. In other words, the local test incorporates to a better extent the network heterogeneities in order to build the null distribution for each connection. The present study was limited to OLS estimates for MVAR, but there exist alternative estimators such as the locally weighted least square regression (Ruppert & Wand, 1994) that may perform better for particular network topologies. The extension of the presented surrogate techniques to the case where observations are sparser than connections—implying that the covariance matrix is not invertible—is another interesting direction to explore (Castelo & Roverato, 2006).

The problem of multiple comparison is intrinsic to brain connectivity detection as the number of testable connections across brain regions is massive (Rubinov & Sporns, 2010). In this context, different approaches have been developed to control the family-wise error rate in the weak sense. For instance, many studies on neuroimaging data (Genovese, Lazar, & Nichols, 2002; Nichols & Hayasaka, 2003) or electrophysiology (Lage-Castellanos, Martínez-Montes, Hernández-Cabrera, & Galán, 2010) have resorted to procedures that control the false discovery rate (FDR) (Benjamini & Hochberg, 1995), namely, the expected number of falsely declared connections among the total number of detections. These methods make decisions on single connections relying on the entire sequence of p values computed for each connection and yield substantial statistical power gains over more conservative methods such as Šidák-Bonferroni (Abdi, 2007). With the ever growing application of graph theory to brain connectivity, new methods have been proposed that exploit the clustered structure of the declared connections (Han, Yoo, Seo, Na, & Seong, 2013; Zalesky, Fornito, & Bullmore, 2010) to propose cluster-based statistical tests (Maris & Oostenveld, 2007) attaining similar performance to FDR methods. The present work can therefore be understood as a primary step before performing any or several multiple-correction procedures. By defining an accurate null model of inexistent connections, p value estimates per connection are improved and cluster-based surrogate distributions can be better approximated, which is expected to empower the overall control of false positive rates in network connectivity analysis.

Applications to Real Electrophysiological and Neuroimaging Data

A motivation for our method is the detection of neuronal interactions between electrode channels, which is often performed using spectral Granger causality analysis on local-field potential (low-passed signal of electrode measurements) or electrocorticography measure-

ments. As an alternative, we have applied our connectivity detection method to MUAe recorded from macaque area V1 in order to provide a proof of concept. Multichannel recording devices have been developed in the past years to obtain this type of data (Fan et al., 2011; Roy & Wang, 2012) and a recent cognitive study has highlighted group properties of MUAe activity for a similar experimental setup to the one used here (Engel et al., 2016). Looking at the variability for individual trials in Figure 8A (upper and middle panels), it is rather surprising that the MUAe conveys temporal information about joint activity for pairs of channels (Figure 8B), which can be related to causal directed interactions. This means that the high trial-to-trial variability is not an absolute limitation to temporal coordination, even though the latter only becomes apparent over multiple trial repetitions, just as the poststimulus increase of MUAe for single channels (lower panel in Figure 8A). The procedure detects a number of significant directional interactions well above the false positive rate that were not merely explained by the MUAe increase (Figures 9D and E). In comparison, the control for the prestimulus period in the four different conditions detects just above the expected false-alarm rate. We find that the parametric Granger causality test also detects many more interactions after the stimulus than before; however, these interactions happen to link channels exhibiting the strongest increases in MUAe activity. This presents the caveat of providing little information in addition to the changes observed at the single-node level, when interpreting the obtained results. The research of optimal preprocessing—in particular the filtering to obtain MUAe—to obtain a robust detection of interactions is left for a later study. Likewise, such electrode recordings are often analyzed with respect to specific frequency bands (e.g., alpha and gamma), but the adaptation of our framework along the lines of previous work (Dhamala et al., 2008; L. Ding et al., 2007) and comparison of detected interactions with established methods will be done in future research.

More generally, our methodology requires adequate preprocessing of multivariate time series—activity aggregation over hundreds of voxels for fMRI and 4-ms smoothing of MUAe for electrode recordings—such that the autocovariance profiles match the exponential decay of the dynamic network model with linear feedback, which underlies the connectivity analysis. Although filtered and smoothed signals fall into the class of autoregressive moving-average (ARMA) models, our approach is applicable provided the autocovariances exhibit a profile resembling Figure 8C. We further expect nonparametric testing methods for be extendable to ARMA processes, complementing approaches developed by Barnett & Seth (2015) and Friston et al. (2014). In theory, stationarity of the time series remains a critical issue as we need sufficiently many observed samples to obtain precise covariances from which we estimate the connectivity, but this may not be a strong limitation for MUAe in practice in view of the poststimulus average response shown in Figure 8A.

ACKNOWLEDGMENTS

The authors are grateful to Robert Castelo and Inma Tur for constructive and inspirational discussions.

AUTHOR CONTRIBUTIONS

Matthieu Gilson: Conceptualization (equal); Formal Analysis; Software; Writing – original Draft (equal). Adriá Tauste Campo: Conceptualization (equal); Formal Analysis (equal); Writing – original Draft (equal). Xing Chen: Investigation. Alexander Thiele: Resources; Writing – original Draft (supporting). Gustavo Deco: Resources; Writing – original Draft (supporting).

FUNDING INFORMATION

MG acknowledges funding from the Marie Skłodowska-Curie Action (grant H2020-MSCA-656547). MG and GD were supported by the Human Brain Project (grant FP7-FET-ICT-604102 and H2020-720270 HBP SGA1). GD and ATC were supported by the European Research Council Advanced Grant DYSTRUCTURE (Grant 295129). AT was supported by the UK Medical Research Council (grant MRC G0700976).

REFERENCES

Abdi, H. (2007). The bonferonni and šidák corrections for multiple comparisons. *Encyclopedia of Measurement and Statistics*, 3, 103–107.

Amemiya, T. (1974). Multivariate regression and simultaneous equation models when the dependent variables are truncated normal. *Econometrica: Journal of the Econometric Society*, 42(6), 999–1012.

Babiloni, F., Cincotti, F., Babiloni, C., Carducci, F., Mattia, D., Astolfi, L., . . . He, B. (2005). Estimation of the cortical functional connectivity with the multimodal integration of high-resolution EEG and fMRI data by directed transfer function. *Neuroimage*, 24(1), 118–131.

Barnett, L., & Seth, A. (2014). The MVGC multivariate Granger causality toolbox: A new approach to Granger-causal inference. *Journal of Neuroscience Methods*, 223, 50–68.

Barnett, L., & Seth, A. (2015). Granger causality for state-space models. *Physical Review E*, 91, 040101. <https://doi.org/10.1103/PhysRevE.91.040101>

Barrett, A., & Barnett, L. (2013). Granger causality is designed to measure effect, not mechanism. *Frontiers in Neuroinformatics*, 7, 6. <https://doi.org/10.3389/fninf.2013.00006>

Benjamini, Y., & Hochberg, Y. (1995). Controlling the false discovery rate: A practical and powerful approach to multiple testing. *Journal of the Royal Statistical Society. Series B (Methodological)*, 289–300.

Castelo, R., & Roverato, A. (2006). A robust procedure for Gaussian graphical model search from microarray data with p larger than n . *The Journal of Machine Learning Research*, 7, 2621–2650. Retrieved from <http://dl.acm.org/citation.cfm?id=1248641>

Cortex [Computer software]. Laboratory of Neuropsychology, NIMH. <http://dally.nimh.nih.gov/index.html>

Dhamala, M., Rangarajan, G., & Ding, M. (2008). Analyzing information flow in brain networks with nonparametric Granger causality. *NeuroImage*, 41(2), 354–362.

Diks, C., & DeGoede, J. (2001). A general nonparametric bootstrap test for Granger causality. In Bernd Krauskopf, Henk W. Broer, & Gert Vegter (Eds.), *Global analysis of dynamical systems* (pp. 391–403). Bristol, UK: Institute of Physics Publishing.

Ding, L., Worrell, G., Lagerlund, T., & He, B. (2007). Ictal source analysis: Localization and imaging of causal interactions in humans. *NeuroImage*, 34(2), 575–586.

Ding, M., Chen, Y., & Bressler, S. (2006). Granger causality: Basic theory and application to neuroscience. In B. Schelter, M. Winterhalder, & J. Timmer (Eds.), *Handbook of time series analysis: Recent theoretical developments and applications*. arXiv preprint q-bio/0608035: Wiley-VCH Verlag.

Engel, T. A., Steinmetz, N. A., Gieselmann, M. A., Thiele, A., Moore, T., & Boahen, K. (2016). Selective modulation of cortical state during spatial attention. *Science*, 354, 1140–1144.

Faes, L., Marinazzo, D., Montalto, A., & Nollo, G. (2014). Lag-specific transfer entropy as a tool to assess cardiovascular and cardiorespiratory information transfer. *IEEE Transactions on Biomedical Engineering*, 61, 2556–2568. <https://doi.org/10.1109/TBME.2014.2323131>

Fan, D., Rich, D., Holtzman, T., Ruther, P., Dalley, J. W., Lopez, A., . . . Yin, H. H. (2011). A wireless multi-channel recording system for freely behaving mice and rats. *PLoS ONE*, 6, e22033.

Friston, K., Bastos, A., Oswal, A., van Wijk, B., Richter, C., & Litvak, V. (2014). Granger causality revisited. *NeuroImage*, 101, 796–808. <https://doi.org/10.1016/j.neuroimage.2014.06.062>

Friston, K., Harrison, L., & Penny, W. (2003). Dynamic causal modelling. *NeuroImage*, 19(4), 1273–1302.

Genovese, C., Lazar, N., & Nichols, T. (2002). Thresholding of statistical maps in functional neuroimaging using the false discovery rate. *NeuroImage*, 15(4), 870–878.

Geweke, J. (1982). Measurement of linear dependence and feedback between multiple time series. *Journal of the American Statistical Association*, 77, 304–313.

Geweke, J. (1984). Measures of conditional linear dependence and feedback between time series. *Journal of the American Statistical Association*, 79, 907–915.

Granger, C. (1969). Investigating causal relations by econometric models and cross-spectral methods. *Econometrica: Journal of the Econometric Society*, 424–438.

Han, C., Yoo, S., Seo, S., Na, D., & Seong, J.-K. (2013). Cluster-based statistics for brain connectivity in correlation with behavioral measures. *PLoS ONE*, 8(8), e72332.

Kaminski, M., & Blinowska, K. (1991). A new method of the description of the information flow in the brain structures. *Biological Cybernetics*, 65(3), 203–210.

Kamiński, M., Ding, M., Truccolo, W., & Bressler, S. (2001). Evaluating causal relations in neural systems: Granger causality, directed transfer function and statistical assessment of significance. *Biological Cybernetics*, 85(2), 145–157.

Lage-Castellanos, A., Martínez-Montes, E., Hernández-Cabrera, J., & Galán, L. (2010). False discovery rate and permutation test: An evaluation in ERP data analysis. *Statistics in Medicine*, 29(1), 63–74.

Li, Y., Ye, X., Liu, Q., Mao, J., Liang, P., Xu, J., & Zhang, P. (2016). Localization of epileptogenic zone based on graph analysis of stereo-EEG. *Epilepsy Research*, 128, 149–157.

Downloaded from <http://direct.mit.edu/net/article-pdf/14/3/371/1091872> on 09 February 2024

- Lusch, B., Maia, P., & Kutz, J. (2016). Inferring connectivity in networked dynamical systems: Challenges using Granger causality. *Physical Review E*, *94*, 032220.
- Lütkepohl, H. (2005). *New introduction to multiple time series analysis*. Berlin: Springer Science & Business Media.
- Maris, E., & Oostenveld, R. (2007). Nonparametric statistical testing of EEG- and MEG-data. *Journal of Neuroscience Methods*, *164*(1), 177–190.
- Massey, J. (1990). Causality, feedback and directed information. *Proceedings ISITA 1990 International Symposium*, 303–305.
- Messé, A., Rudrauf, D., Benali, H., & Marrelec, G. (2014). Relating structure and function in the human brain: Relative contributions of anatomy, stationary dynamics, and non-stationarities. *PLoS Computational Biology*, *10*, e1003530.
- Michalareas, G., Schoffelen, J., Paterson, G., & Gross, J. (2013). Investigating causality between interacting brain areas with multivariate autoregressive models of MEG sensor data. *Human Brain Mapping*, *34*(4), 890–913. <https://doi.org/10.1002/hbm.21482>
- Nedungadi, A., Rangarajan, G., Jain, N., & Ding, M. (2009). Analyzing multiple spike trains with nonparametric Granger causality. *Journal of Computational Neuroscience*, *27*(1), 55–64.
- Nichols, T., & Hayasaka, S. (2003). Controlling the familywise error rate in functional neuroimaging: A comparative review. *Statistical methods in medical research*, *12*(5), 419–446.
- Rogers, B., Katwal, S., Morgan, V., Asplund, C., & Gore, J. (2010). Functional MRI and multivariate autoregressive models. *Magnetic Resonance Imaging*, *28*(8), 1058–1065.
- Roy, S., & Wang, X. (2012). Wireless multi-channel single unit recording in freely moving and vocalizing primates. *Journal of Neuroscience Methods*, *203*, 28–40.
- Rubinov, M., & Sporns, O. (2010). Complex network measures of brain connectivity: Uses and interpretations. *NeuroImage*, *52*(3), 1059–1069.
- Ruppert, D., & Wand, M. (1994). Multivariate locally weighted least squares regression. *Annals of Statistics*, *22*, 1346–1370.
- Schreiber, T. (1998). Constrained randomization of time series data. *Physical Review Letters*, *80*, 2105.
- Schreiber, T. (2000). Measuring information transfer. *Physical Review Letters*, *85*, 461.
- Schreiber, T., & Schmitz, A. (1996). Improved surrogate data for nonlinearity tests. *Physical Review Letters*, *77*, 635.
- Scientific Python Library. (n.d.). <http://www.scipy.org>
- Seth, A., Barrett, A., & Barnett, L. (2015). Granger causality analysis in neuroscience and neuroimaging. *Journal of Neuroscience*, *35*, 3293–3297. <https://doi.org/10.1523/JNEUROSCI.4399-14.2015>
- So, K., Koralek, A., Ganguly, K., Gastpar, M., & Carmena, J. (2012). Assessing functional connectivity of neural ensembles using directed information. *Journal of Neural Engineering*, *9*(2), 026004.
- Sporns, O. (2013). Making sense of brain network data. *Nature Methods*, *10*, 491–493.
- Storkey, A., Simonotto, E., Whalley, H., Lawrie, S., Murray, L., & Mcgonigle, D. (2007). Learning structural equation models for fMRI. In B. Schölkopf, J. Platt, & T. Hoffman (Eds.), *Advances in neural information processing systems 19* (pp. 1329–1336). Cambridge, MA: MIT Press.
- Stramaglia, S., Cortes, J., & Marinazzo, D. (2014). Synergy and redundancy in the Granger causal analysis of dynamical networks. *New Journal of Physics*, *16*, 105003.
- Supèr, H., & Roelfsema, P. (2005). Chronic multiunit recordings in behaving animals: Advantages and limitations. *Progress in Brain Research*, *147*, 263–282.
- Tauste Campo, A., Martinez-Garcia, M., Nácher, V., Luna, R., Romo, R., & Deco, G. (2015). Task-driven intra- and inter-area communications in primate cerebral cortex. *Proceedings of the National Academy of Sciences*, *112*(15), 4761–4766.
- Thiele, A., Delicato, L., Roberts, M., & Gieselmann, M. (2006). A novel electrode-pipette design for simultaneous recording of extracellular spikes and iontophoretic drug application in awake behaving monkeys. *Journal of Neuroscience Methods*, *158*, 207–211.
- Vinck, M., Hurdeman, L., Bosman, C., Fries, P., Battaglia, F., Pennartz, C., & Tiesinga, P. (2015). How to detect the Granger-causal flow direction in the presence of additive noise? *NeuroImage*, *108*, 301–318. <http://doi.org/10.1016/j.neuroimage.2014.12.017>
- Wilke, C., Ding, L., & He, B. (2008). Estimation of time-varying connectivity patterns through the use of an adaptive directed transfer function. *IEEE Transactions on Biomedical Engineering*, *55*(11), 2557–2564.
- Winkler, A., Ridgway, G., Webster, M., Smith, S., & Nichols, T. (2014). Permutation inference for the general linear model. *NeuroImage*, *92*, 381–397. <https://doi.org/10.1016/j.neuroimage.2014.01.060>
- Zalesky, A., Fornito, A., & Bullmore, E. (2010). Network-based statistic: Identifying differences in brain networks. *NeuroImage*, *53*(4), 1197–1207.